Chemical Science

ROYAL SOCIETY OF CHEMISTRY

EDGE ARTICLE

View Article Online
View Journal

Cite this: DOI: 10.1039/d6sc00926c

All publication charges for this article have been paid for by the Royal Society of Chemistry

Flexible dimethylsilylene bridges in silicon quantum dot-anthracene adducts promote triplet energy transfer

Sina G. Lewis, †[b] Kefu Wang, †[c] Nhien Q. Nguyen,†[a] Aracely Gonzalez,[a] Honghao Wang,[d] Timothy C. Siu,[a] Lorenzo Mangolini,[e] Sean T. Roberts,[d] Timothy A. Su, *[a] Joel David Eaves*[f] and Ming Lee Tang *[c]

Triplet energy transfer (TET) underlies key applications in energy storage, conversion, and utilization such as photovoltaics, photon upconversion, singlet fission, and photocatalysis. Fast and long-distance TET is generally desirable in these applications to enhance performance and limit back transfer. However, conventional TET in the weak coupling regime only occurs over short distances between donor and acceptor as Dexter-type electronic coupling for TET decreases exponentially with increasing separation. One way to achieve long-distance TET is to enhance the electronic coupling between donor and acceptor by designing conjugated linking bridges. Here, we reveal three new silicon quantum dot (Si QD):Anthracene hybrid systems with variable-length $-[SiMe_2]_n-$ ($n = 2$–4) linkers as bridges to promote long-distance TET. Transient absorption experiments and density functional theory calculations show that electronic coupling in each of these four systems is intermediate between non-conjugated ethyl and π-conjugated vinyl bridges. In addition, the TET rates between Si QDs and anthracene facilitated by $-[SiMe_2]_n-$ ($n = 1$–4) linkers do not show the expected exponential decay trend with increasing separation. Rather we observe an increase in the rate of TET when n is increased from 2 to 3, which we propose arises from greater bridge chain flexibility that opens access to geometries where the anthracene can directly engage the Si QD surface *via* through-space van der Waals interactions. By controlling the average number of tethered anthracene transmitters, we are able to optimize the performance of Si QD:Anthracene hybrids as photosensitizers for triplet–triplet annihilation photon upconversion, obtaining efficiencies of 6.2 ± 0.4%, 3.4 ± 0.1%, 4.1 ± 0.2% and 3.9 ± 0.1% (out of 100%), respectively for $n = 1$–4. This work provides insight into the role that electronic coupling plays in hybrid materials to move triplet excitons across semiconductor junctions, which sheds light on material design principles for applications in optoelectronics and photocatalysis.

Received 2nd February 2026
Accepted 5th April 2026

DOI: 10.1039/d6sc00926c

rsc.li/chemical-science

Introduction

Triplet energy transfer (TET) plays a crucial role in processes like photocatalysis, singlet fission, and photon upconversion[1–3] where rapid, directed TET over long distances is desirable. In triplet–triplet annihilation (TTA)-based photon upconversion, fast, unidirectional TET between a donor and acceptor contributes to a higher photon upconversion efficiency with lower excitation power.[4–6] In singlet fission, fast TET facilitates rapid separation of triplet pairs to prevent geminate recombination, thus producing two excitons from one photon.[7,8] However, conventional TET is limited to short distances because it obeys a Dexter energy transfer mechanism, which often features an effective transfer radius of about 1 nm that rapidly decays with increasing donor–acceptor distance.[9] The ability to improve both the rate and efficacy of TET by tuning steric and electronic factors motivates this work.

We recently established that the electronic coupling between silicon quantum dot (Si QD) donors and tethered anthracene triplet acceptors can be tuned by modulating the chemical structure of their bridging units.[10,11] Weak and intermediate coupling resulted from saturated methylene and $Si(CH_3)_2$ bridges, respectively, while strong electronic coupling was observed with sp^2 hybridized C=C bonds between the Si QDs and attached anthracene. In weakly-coupled Si QD:Anthracene

[a]Department of Chemistry, University of California Riverside, Riverside, USA. E-mail: minglee.tang@utah.edu; timothys@ucr.edu
[b]Department of Physics, University of Colorado Boulder, Boulder, USA
[c]Department of Chemistry, University of Utah, Salt Lake City, USA
[d]Department of Chemistry, The University of Texas at Austin, Austin, USA
[e]Department of Mechanical Engineering, University of California Riverside, Riverside, USA
[f]Department of Chemistry, University of Colorado Boulder, Boulder, USA. E-mail: Joel.Eaves@colorado.edu
† These authors contributed equally.

hybrid systems, the rate of TET from QD donor to attached anthracene acceptors is governed by the driving force for energy transfer. Experimentally, a TET time constant of ~15 ns is observed when the QD photoluminescence maxima, a proxy for the QD bandgap, is resonant with the triplet acceptor state. In contrast, in strongly-coupled systems bridged by vinyl groups, the excitonic wavefunctions of the QD significantly mixes with the attached molecules, resulting in delocalized excitonic states over the inorganic nanocrystal and organic chromophore. This strong coupling reduces the TET time constant to 3 ns. For Si QDs bridged by $SiMe_2$ (Fig. 1a) to anthracene, the electronic coupling strength falls between the weakly-coupled and strongly-coupled systems and TET unfolds with a slower rate than that seen in the case of strong coupling.[11] These variations highlight the critical role played by the structure of the bridge in gating the electronic coupling between QD donors and molecular acceptors during TET.

Over the course of our prior studies,[11] a key question that emerged was how increasing the oligosilane chain length influences both triplet energy transfer between a Si QD and anthracene ligands and the system's resulting ability to facilitate TTA-based photon upconversion. It is well-understood that in the tunneling regime the rate of triplet transfer decays exponentially with increasing molecular length. The attenuation factor β is typically shallower for bridging units that experience stronger electronic coupling. Extracting the β value thus provides a metric that characterizes the fundamental efficiency with which oligomeric bridges mediate triplet energy transfer. Previously, we have explored the triplet transfer rate and photon upconversion quantum yield as a function of *para*-phenylene bridges between CdSe QDs and anthracene transmitters.[12,13] We found that depending on the end group binding the oligophenylene to the QD, $\beta = 0.43–0.72$ Å^{-1}. Meanwhile, efforts to investigate methylene spacers in photoinduced electron transfer from QDs have revealed steeper β values for alkanes,[14] although in other systems, the flexibility of the alkane chain allows the bridge to backbite in such a way that the terminal acceptor can directly engage the QD through van der Waals interactions, leading the transfer rate to be approximately the same, regardless of the alkane chain length of the bridge.[12,15]

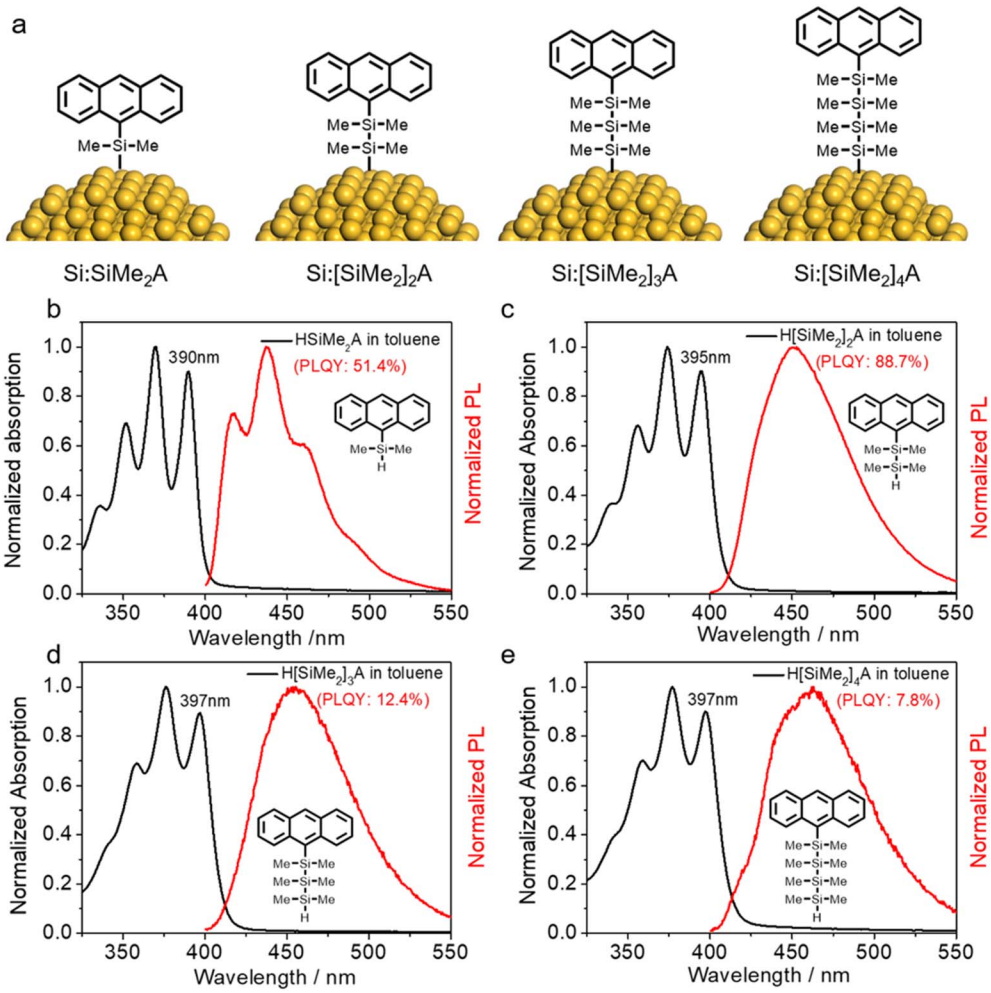

Fig. 1 (a) Si:$[SiMe_2]_nA$ ($n = 1–4$) hybrid structures with increasing lengths of dimethylsilylene bridging units between the Si QD and anthracene transmitter; (b–e) absorption and photoluminescence spectra of $HSiMe_2A$, $H[SiMe_2]_2A$, $H[SiMe_2]_3A$ and $H[SiMe_2]_4A$ molecules in toluene at room temperature (excitation at 375 nm).

In addition, tunneling electronic transport through alkanes, oligosilanes, and phenylenes in conductive single-molecule junctions have revealed that, on a per length basis, oligosilanes have a similar inverse conductance decay value as oligophenylenes.[16,17] However, similar to alkanes, oligosilanes have conformationally flexible tetrahedral σ-bonds that may be similarly capable of the backbiting characteristic of alkanes.[18] Meanwhile, it has been shown that long oligosilane chains experience strong stereoelectronic effects upon dihedral chain twisting that profoundly influence their molecular orbital properties compared to alkanes.[19,20] We wanted to explore these implications in the context of TET.

Here we investigate four Si QD donor/anthracene acceptor hybrids that are linked by dimethylsilylene chains of increasing oligomer length (Si:[$SiMe_2$]$_n$A, n = 1–4, Fig. 1a). The surface-bound anthracene ligands, [$SiMe_2$]$_n$A, serve to transmit energy from a Si QD triplet photosensitizer to 9,10-diphenylanthracene (DPA) emitters for TTA-based photon upconversion. The photon upconversion QY under steady-state conditions with CW excitation is a proxy for the efficiency and rate of TET, the latter experimentally obtained *via* nanosecond transient absorption spectroscopy. These hybrid systems show an intermediate electronic coupling strength between the Si QD and anthracene acceptor, compared to the previously reported Si:[CH_2CH_2]A (*i.e.,* Si:9EA): and Si:[CH═CH]A (*i.e.*, Si:9VA): systems, as inferred by their triplet excited state absorption and lifetime trends. The best photon upconversion quantum yields of the Si:[$SiMe_2$]$_n$A (n = 1–4) hybrid systems with DPA emitters were 6.2%, 3.4%, 4.1%, 3.9% for n = 1–4 respectively, out of a maximum of 100%. Notably, both the photon upconversion efficiency and the triplet transfer rate decreased upon lengthening the bridge from one to two $SiMe_2$ units, but a slight increase followed by a plateau is observed as the bridge length was further increased. This outcome is unexpected as the rate of triplet transfer should exponentially decay with increasing distance. From classical molecular dynamics simulations, this deviation from the Dexter model of energy transfer can be attributed to both the torsional flexibility and electronic structure of the dimethylsilylene bridge, which may provide a viable means to promote long-distance triplet energy transfer for optoelectronic applications.

Results

The transmitter molecules (H[$SiMe_2$]$_n$A, n = 1–4, Fig. 1a) were synthesized for dehydrocoupling attachment onto H-terminated Si QDs (see SI for synthetic details). Fig. 1b–e plot the absorption and photoluminescence (PL) spectra of these anthracene molecules in toluene. All show the typical vibrational fine structure of the $S_0 \rightarrow S_1$ transition corresponding to anthracene absorption between 300–400 nm.[21] The absorption maxima of $HSiMe_2$A is located at 390 nm. This peak redshifts to 395 nm for H[$SiMe_2$]$_2$A and 397 nm for both H[$SiMe_2$]$_3$A and H[$SiMe_2$]$_4$A. This redshift suggests increased conjugation between the –$SiMe_2$ bridge and anthracene core as more Si atoms are added. As seen in Fig. 1b, the PL spectrum of $HSiMe_2$A shows the vibrational fine structure associated with anthracene fluorescence. However, for H[$SiMe_2$]$_2$A, H[$SiMe_2$]$_3$A and H[$SiMe_2$]$_4$A, the PL peak broadens and loses its fine structure, suggesting the oligosilane chain is conformationally flexible.[20] The fluorescence quantum yields of $HSiMe_2$A, H[$SiMe_2$]$_2$A, H[$SiMe_2$]$_3$A and H[$SiMe_2$]$_4$A were measured to be 51.4%, 88.7%, 12.4%, 7.8%, respectively, using DPA in toluene (fluorescence QY of 90%) as a standard.[22]

These trends in diminishing quantum yield and loss in fine vibronic structure with increasing oligosilane chain length broadly match previously reported fluorescence trends for increasing dimethylsilylene order in α, ω-dinapthyloligosilanes and α, ω-dianthracenyloligosilanes.[23,24] Quantum yields in oligosilanes generally decrease as chain length increases. The greater conformational flexibility introduces additional non-radiative decay pathways as chain dihedrals rotate between *transoid*, *ortho*, and *gauche* states. However, it has also been observed that aryldisilanes typically have high quantum yields, presumably because the emergent delocalized Si–Si bond enables a strong σ–π interaction, yet is not long enough to possess discrete *transoid*, *ortho*, and *gauche* –Si–Si–Si–R– orientations that would otherwise contribute to non-radiative decay.[25] These considerations may rationalize why the PLQY increases from the monosilane to the disilane, but continues to decrease for the trisilane and tetrasilane.

A non-thermal plasma was employed to prepare Si QDs with SiH_4 and H_2 gas as precursors.[26] During the synthesis, as part of the surface functionalization, 1-dodecene vapor was introduced into the plasma reactor with a H_2 carrier gas immediately after the formation of Si QDs, to yield dodecane-capped Si QDs (Si:dodecane) that were soluble in hydrophobic solvents for subsequent functionalization with transmitter molecules (see SI for details). As shown in Fig. S1, previously reported methods using AIBN radical initiators[27,28] or high-temperature heating failed to attach these silane-functionalized anthracenes to the Si QDs, as no anthracene features were observed after the reaction.

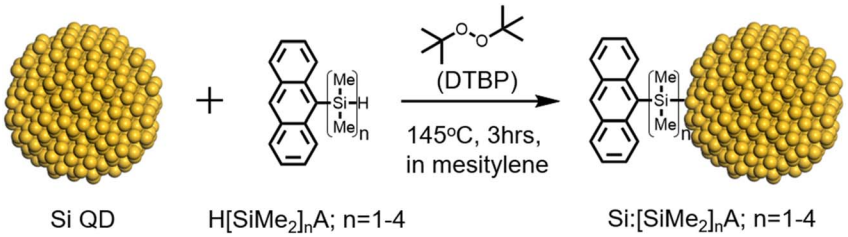

Scheme 1 Surface functionalization of Si QDs with H[$SiMe_2$]$_n$A (n = 1–4) using di-*tert*butylperoxide (DTBP) as a radical initiator.

As shown in Scheme 1, the Si QDs, dimethylsilylene-anthracene precursors, and the di-*tert*butylperoxide (DTBP) radical initiator were dissolved in mesitylene and heated at 145 °C for 3 hours, generating Si QDs functionalized with a mixture of 1-dodecane and –[$SiMe_2$]$_n$– anthracene ligands (denoted here as Si:[$SiMe_2$]$_n$A, n = 1–4). After the reaction, the Si QD:anthracene hybrids were separated from the unbound molecules and dimerization side products by repeated centrifugation and re-dispersion steps (see SI for details).

Electronic absorption spectra measured after the reaction confirm successful attachment of dimethylsilylene–anthracene molecules to Si QDs. Fig. 2 shows the absorption spectra of Si:dodecane and Si:[$SiMe_2$]$_n$A (n = 1–4) with different amounts of transmitter molecules on the QD surface. The featureless character of the Si:dodecane absorption spectrum reflects the Si QDs' indirect bandgap. In contrast, Si:[$SiMe_2$]$_n$A absorption spectra display a series of peaks near 400 nm assigned to anthracene-centered transitions. These bands grow as the surface coverage of transmitter molecules increases. Comparison of the amplitude of these bands to extinction spectra of $HSiMe_2A$ indicates that $\langle N_{SiMe_2A}\rangle$, the average number of anchored anthracenes per Si QD, varies from 0.4 to 4.1 depending on the amount of $HSiMe_2A$ added to the functionalization reaction. The higher-order oligosilane bridges fall within similar ranges, where $\langle N_{[SiMe_2]2A}\rangle$ = 0.8–2.4, $\langle N_{[SiMe_2]3A}\rangle$ = 0.9–3.1, and $\langle N_{[SiMe_2]4A}\rangle$ = 0.8–3.2 (see SI for more detail).

Photon upconversion measurements of Si:[$SiMe_2$]$_n$A (n = 1–4) systems were conducted with DPA emitters in toluene at room temperature under nitrogen atmosphere. During photon upconversion, the Si QDs absorb low-energy photons, creating bright excitons with spin-singlet character that equilibrate with dark excitons.[29] These triplet-like, dark excitons at the band edge can photosensitize surface-bound anthracene transmitters. The triplet excitons in anthracene transmitters are transferred down an energy gradient to emitter molecules diffusing in solution. When two emitters undergo triplet–triplet annihilation, one molecule returns to its ground state while the other is promoted to its lowest-energy spin-singlet excited state. Fluorescence from this singlet excited state results in photon upconversion.

To measure the photon upconversion quantum yield, diluted DPA in toluene (10 μM) was employed as an emission standard (See SI). For the Si:dodecane system without anthracene transmitters, the photon upconversion quantum yield was negligible (<0.4%), which is reasonable since the long dodecane ligands present a formidable barrier for triplet energy transfer from a Si QD to a DPA emitter if there is no molecular transmitter. Fig. 3 shows emission spectra of the hybrid Si:[$SiMe_2$]$_n$A sensitizers in 5.2 mM DPA in toluene under 488 nm CW irradiation that excites the Si QDs, but not anthracene. The emission seen at 700−800 nm is attributed to Si QD PL and the peak between 400−500 nm corresponds to photon upconverted emission from DPA. Interestingly, for all Si:[$SiMe_2$]$_n$A (n = 1–4), photon

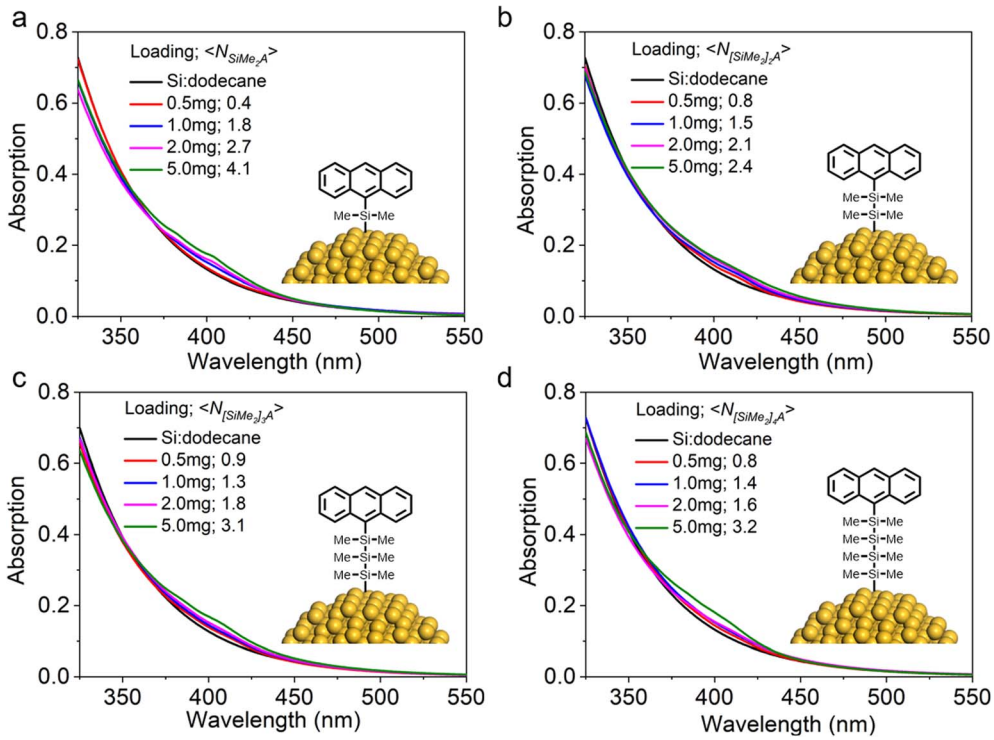

Fig. 2 Absorption spectra of (a) Si:$SiMe_2$A, (b) Si:[$SiMe_2$]$_2$A, (c) Si:[$SiMe_2$]$_3$A, and (d) Si:[$SiMe_2$]$_4$A in toluene at room temperature (loading: amount of dimethylsilylene–anthracene added for reaction with Si QDs, $HSiMe_2A$ for Si:$SiMe_2$A, H[$SiMe_2$]$_2$A for Si:[$SiMe_2$]$_2$A, H[$SiMe_2$]$_3$A for Si:[$SiMe_2$]$_3$A, and H[$SiMe_2$]$_4$A for Si:[$SiMe_2$]$_4$A; $\langle N_{[SiMe_2]nA}\rangle$: the average number of attached anthracenes per Si QD). The molecular vibrational fine structure around 400 nm is typical for anthracene absorption, indicating the successful attachment of anthracenes to Si QDs.

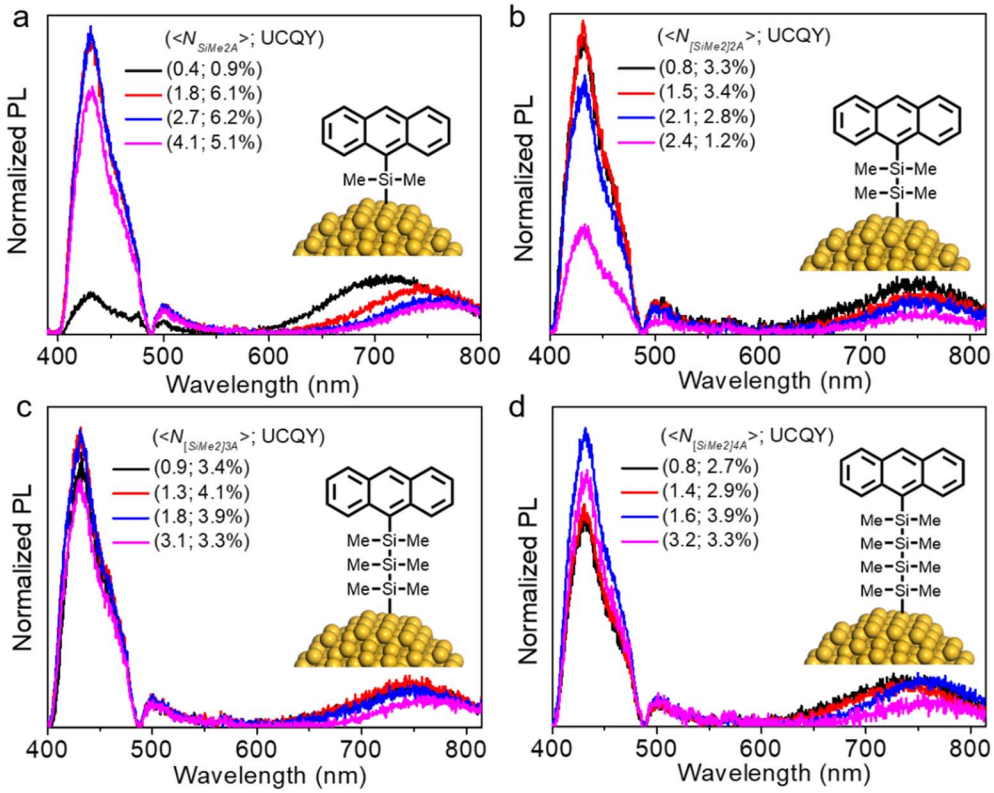

Fig. 3 Upconversion emission spectra of (a) Si:$SiMe_2$A, (b) Si:$[SiMe_2]_2$A, (c) Si:$[SiMe_2]_3$A and (d) Si:$[SiMe_2]_4$A generated by Si QDs functionalized with differing numbers of anthracene ligands, $<N_{[SiMe_2]nA}>$. Spectra were collected using DPA emitters (5.2 mM) in toluene, exciting each system with a CW 488 nm laser at RT.

upconversion quantum yields increased with more surface bound anthracene up to a point, reaching a maximum beyond which the upconversion quantum yield dropped as the anthracene loading grew. The optimized photon upconversion efficiencies for Si:$[SiMe_2]_n$A (n = 1–4) with DPA emitters (all values are out of 100% maximum) were 6.2%, 3.4%, 4.1%, and 3.9%, respectively. The photon upconversion quantum yield was the highest for the transmitter ligand with one dimethylsilylene unit, then dropped by a factor of 2 to between 3.4−4.1% for the other 3 ligands. This trend is unexpected, as the triplet transfer rate from Si QDs to anchored anthracene should decrease exponentially with increasing distance between donor and acceptor if governed solely by Dexter energy transfer.

To identify rates of triplet exciton formation in these systems, we performed transient absorption (TA) measurements over both femtosecond and nanosecond time scales. Femtosecond measurements that photoexcited the Si QDs in each hybrid system showed dynamics consistent with exciton cooling over femtosecond-to-picosecond timescales that were independent of the QDs' ligand shell composition (Fig. S5). In contrast, features signaling Si QD-to-anthracene TET were observed in TA measurements that employed nanosecond-to-microsecond delays (Fig. 4). Following photoexcitation of the Si QDs by a 532 nm nanosecond pulse, a broad induced absorption in the NIR region is seen for each of the Si:$[SiMe_2]_n$A (n = 1–4) hybrids that is characteristic of the Si QD excited state absorption (ESA).[10,21,30–34] Over time, this band relaxes over the course of a few tens of nanoseconds concomitant with the growth of an induced absorption band peaked around ~450 nm that corresponds to the triplet ($T_1 \rightarrow T_n$) ESA of attached anthracene molecules in Si:$[SiMe_2]_n$A (n = 1–4). As the 532 nm laser used for these measurements only excites the Si QDs, not the attached anthracene molecules, the anthracene triplet ESA signal must arise from triplet transfer from photoexcited Si QDs, thus confirming TET occurs during photon upconversion.

TA measurements were also performed to identify the triplet absorption spectra of free anthracene monomers (H$[SiMe_2]_n$A, n = 1–4) *via* sensitization experiments that employed Pt(II) octaethylporphyrin (PtOEP) as a triplet sensitizer (Fig. S4). As time evolves in these measurements, for each H$[SiMe_2]_n$A molecule we observe broad positive features centered between 430 – 435 nm that appear concomitantly with the decay of TA features associated with PtOEP's T_1 state, which we assign to their $T_1 \rightarrow T_n$ absorption. Comparing these spectra to the $T_1 \rightarrow T_n$ absorption features seen in TA measurements of the Si:$[SiMe_2]_n$A hybrids reveals that attachment of the H$[SiMe_2]_n$A to a Si QD induces a redshift of their triplet absorption bands. This shift takes on values of 15 nm, 7.5 nm, 17.5 nm and 20 nm respectively as n increases from 1 to 4 (Fig. 5). This redshift between free and anchored anthracenes on Si QDs directly correlates with the strength of the electronic coupling between surface-bound anthracene and Si QDs, and the values seen for

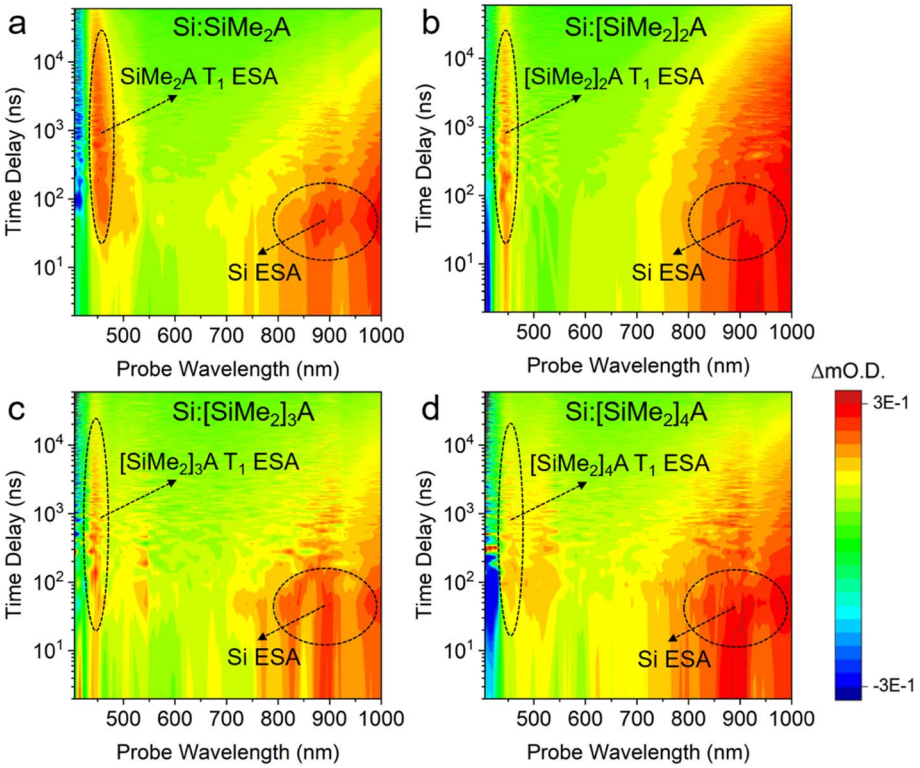

Fig. 4 (a–d) TA spectra of Si:$SiMe_2$A, Si:$[SiMe_2]_2$A, Si:$[SiMe_2]_3$A, and Si:$[SiMe_2]_4$A in toluene at room temperature, recorded following excitation at 532 nm. The induced absorption around 450 nm (red/orange) in Si:$[SiMe_2]_n$A (n = 1–4) corresponds to the $T_1 \rightarrow T_n$ absorption of anchored anthracenes, confirming TET after photoexcitation of the Si QD. Data reported for Si:$SiMe_2$A originally appeared in ref. 11.

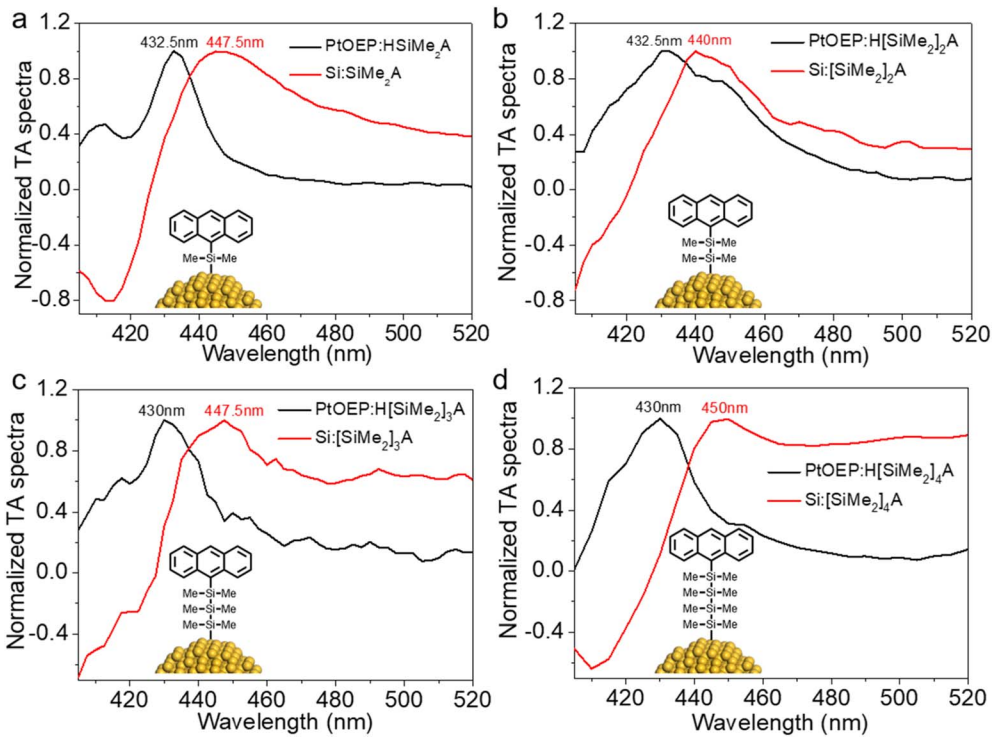

Fig. 5 Comparison of the triplet ESA of H$[SiMe_2]_n$A measured *via* PtOEP sensitization (black) and TA spectra of Si:$[SiMe_2]_n$A measured at a time delay of 25 μs (red): (a) $SiMe_2$A, (b) $[SiMe_2]_2$A, (c) $[SiMe_2]_3$A and (d) $[SiMe_2]_4$A. The shift of the triplet absorption band between these spectra reflects the strength of the electronic coupling between Si QDs and anchored anthracenes. Data reported for Si:$SiMe_2$A originally appeared in ref. 11.

Si:[$SiMe_2$]$_n$A are larger than that of the weakly coupled Si:9 EA system (2.5 nm), but smaller than that of the strongly coupled Si:9VA system (55 nm).[10,11,21] Thus, the electronic couplings in the Si:[$SiMe_2$]$_n$A (n = 1–4) hybrid systems are intermediate to those seen in Si:9 EA and Si:9VA.

Kinetic traces describing the growth of the anthracene triplet state following photoexcitation of the Si:[$SiMe_2$]$_n$A (n = 1–4) hybrid systems were extracted from the TA spectra (Fig. S6 & S7). The triplet population for each system was found to reach a maximum after a few tens of nanoseconds. A single exponential fitting function was employed to fit the triplet kinetics to obtain the triplet transfer time constants from Si QDs to anchored anthracenes, which were found to be 24.2 ± 3.0 ns, 92 ± 43 ns, 42 ± 9 ns, and 33 ± 11 ns for Si:$SiMe_2$A, Si:[$SiMe_2$]$_2$A, Si:[$SiMe_2$]$_3$A, and Si:[$SiMe_2$]$_4$A, respectively. Interestingly, the triplet transfer times do not lengthen as more dimethylsilylene units are introduced into the bridge. This is unexpected as lengthening the dimethylsilyene bridge should exponentially slow the TET rate according to Dexter's model.[35] We note this trend holds even when accounting for variations in the average number of ligands that bind to the Si QDs in each sample (See SI, Section II.6).

To visualize how the photon upconversion and triplet transfer rate evolve from Si:$SiMe_2$A to Si:[$SiMe_2$]$_4$A, we plotted the photon upconversion quantum yields and triplet transfer rates *versus* n, the number of repeating dimethylsilylene units for Si:[$SiMe_2$]$_n$A (n = 1–4) (Fig. 6). Notably, the photon upconversion quantum yield shows a similar trend to the triplet transfer rate as a function of the –[$SiMe_2$]$_n$– bridge length. The efficiency of triplet energy transfer[36,37] from the Si QD to the bound anthracene, ϕ_{TET}, is line with this trend. As n increases from 1 to 2, ϕ_{TET} decreases from 90% to 6.6%, then increases to 61% and drops to 55% for n = 3 and 4 respectively. ϕ_{TET} is extracted from the change in the Si QD time-resolved emission decay with and without the transmitter ligand (Details are provided in SI Section II.7).

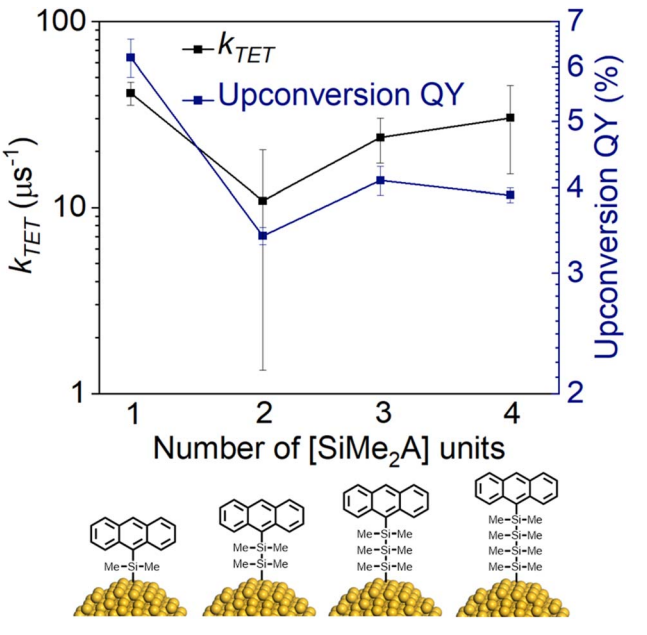

Fig. 6 Triplet transfer rate (black curve) and photon upconversion quantum yield (blue curve) as a function of the dimethylsilyene bridge length connecting Si QDs and anchored anthracenes.

To elucidate the relationship between the dimethylsilane bridge length and the electronic coupling strength, we employed density functional theory (DFT) calculations using methods developed in our previous work.[10,38,39] Briefly, we used semi-periodic boundary conditions on a slab of silicon to model the interface between a Si QD and an anthracene molecule (details in SI Section V Fig. S9 and S10). Using spin-polarized DFT calculations, we obtained the triplet density of states (DOS) for the Si:[$SiMe_2$]$_n$A (n = 1–4) slabs and projected the anthracene molecule's carbon p-orbitals from the triplet DOS. In the DOS, the gap is clear enough to assign electron and hole states. For qualitative analysis, the joint electron–hole DOS, formed by convolving densities above and below the gap, is a surrogate for the triplet exciton DOS (eDOS, Fig. 7a dotted lines). The molecule's p-orbital contribution to the triplet density of states (pDOS, Fig. 7a solid lines) comes from a convolution of the p-orbital projected density of electron and hole states. In the Anderson–Newns model,[40,41] the p-orbitals are quantum impurities that can hybridize with the solid. The extent of broadening in the anthracene's carbon pDOS is proportional to the square of the coupling strength between those orbitals and the solid. The nonadiabatic Dexter theory of the exciton transfer rate is proportional to the same squared coupling strength.[42] The full-width at half-maximum (FWHM) from the pDOS for each system, therefore, measures the excitonic coupling between the molecule and the silicon QD, and should scale as the triplet transfer rate. The FWHM for various linker lengths (Fig. 7b) shows how the electronic coupling strength depends on the linker length. The data show weak dependence of the excitonic coupling strength with increasing n that mirrors the transition from a mechanism based on direct orbital overlap to superexchange-mediated tunneling in theoretical models of donor-bridge-acceptor systems.[43] While the changes in the coupling are small for n = 3, 4—consistent with experimental observations in Fig. 6—the large deviation from the expected trend for n = 2 suggests there is additional physics that needs to be described.

As in our earlier work, the electronic structure calculations do not compute excitonic states using, for example, the Bethe–Salpeter equation, to compute the electron–hole interaction. They also ignore structural fluctuations of the linking groups and the chromophore. In previous work, the differences between the systems under consideration were qualitatively larger than the changes computed here. Additionally, the linking groups were shorter and more rigid, so structural fluctuations were negligible. Therefore, the conclusions were less susceptible to both inaccuracies in the DFT calculations and the neglect of structural fluctuations.

The situation is different here, as both excitonic effects and structural fluctuations are difficult to compute. The number of atoms in the system makes Bethe–Salpeter calculations or time-dependent DFT computationally infeasible, and potentials for molecular dynamics in the molecule-nanocrystal hybrids

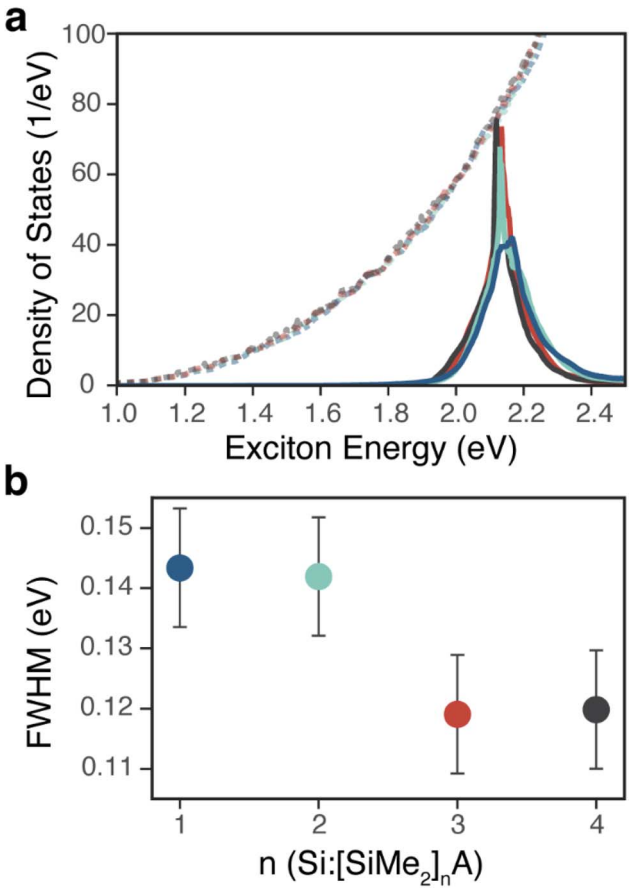

Fig. 7 Exciton density of states analysis of Si:[$SiMe_2$]$_n$A (n = 1–4) systems (blue, teal, red, black, respectively). (a) The silicon states obfuscate the changes from the ligand in the total eDOS (dotted lines). The anthracene's carbon p-orbital contributions to it (pDOS) show resonances that broaden as the coupling between the anthracene π-orbitals and silicon states increases (solid lines, magnified by a factor of 50). (b) The full-width at half-maximum (FWHM) of a Gaussian fit to the main peaks of the pDOS measures the excitonic coupling between anthracene and silicon and should scale as the triplet transfer rate. The FWHM error is dominated by computational convergence, as explained in SI Section V. The disagreement with the experimental trend at n = 2 suggests these static calculations do not capture all necessary physics. Due to the good agreement in our previous work with shorter linker lengths, we elect to explore the effect of structural dynamics.

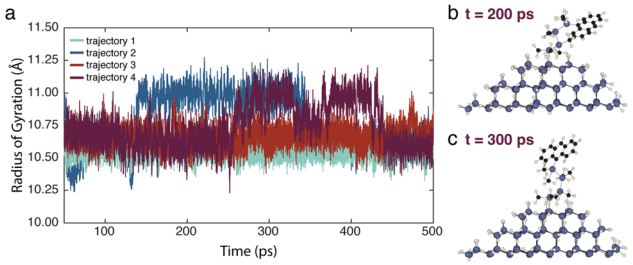

Fig. 8 Classical molecular dynamics for Si:[$SiMe_2$]$_4$A. (a) We ran molecular dynamics at 300 K for 500 ps over four different trajectories, each with a different velocity seed. We describe the extent to which the linker is folded with the radius of gyration (details in the SI). Large jumps indicate a significant change in how the chain is configured. (b) The configuration given by $R_g \approx 10.70$ is achieved during the equilibration stage (not shown) for each of the trajectories. The specific snapshot shown is from t = 200 ps during trajectory 4. For most of the simulations, the linker displays minor fluctuations around this configuration. (c) During trajectory 2 and trajectory 4, the linker spontaneously regains a configuration that is mostly perpendicular to the surface of the Si QD. The snapshot shown is from t = 300 ps during trajectory 4. The majority of the time, the linkers are able to find a configuration that brings the anthracene closer to the surface of the Si QD, leading to stronger coupling and faster triplet exciton transfer than predicted by the zero-temperature DFT calculations. The plotted radius of gyration and representative snapshots for Si:[SiMe2]$_n$A (n = 1–3) are shown in the SI.

presented here are not well-developed compared to other systems. With these limitations in mind, we conducted some calculations using classical molecular dynamics simulations to model structural fluctuations at room temperature for QDs, not slabs. The longer chains, Si:[$SiMe_2$]$_n$:A (n = 3, 4) fold back to the surface or extend into solution as seen for Si:[$SiMe_2$]$_4$:A in Fig. 8b. The extended structures are like those we modeled in DFT at zero Kelvin (Fig. 8c). Additional details and figures for Si:[$SiMe_2$]$_n$:A (n = 1–3) are given in the SI (Fig. S11 and S12). Unfortunately, the calculations of the excitonic coupling are computationally infeasible for folded chains because they require even larger simulations. But anthracene molecules folded to the surface may have a larger triplet transfer rate than those extended into the solution, simply because they are closer to the surface. For n = 3, 4, the folded configurations may be responsible for the relative increase in the triplet transfer rate and upconversion QY observed in Fig. 6.

Finally, we note this oligosilane chain-folding model that may rationalize the flat k_{TET} and UCQY trends we observe is consistent with proposals by others who have studied photoinduced electron transfer across permethyloligosilane bridges. Ito, Tamao, and coworkers investigated photoinduced electron transfer across permethyloligosilane ([$SiMe_2$]$_n$, n = 1–5) bridges in C_{60}-oligosilane-zinc porphyrin dyads.[15,44,45] Similar to our observations here, these authors did not find a linear trend in charge recombination rate or radical-ion pair lifetime with increasing oligosilane bridge length, finding a flat trend in both cases. These plateaus in lifetime and rate were attributed to combinations of extended, chain length-dependent through-bond interactions and folded, chain length-independent through-space interactions between the C_{60} and zinc porphyrin termini; these states coexist due to the flexible nature of the oligosilane chain. As the same permethyloligosilane chains are involved in the bridges here, we are likely seeing similar conformational effects.

Conclusions

In summary, a series of H-[$SiMe_2$]$_n$-anthracene (n = 1–4) transmitter molecules were synthesized and successfully attached to Si QDs to form Si:[$SiMe_2$]$_n$A (n = 1–4) hybrid structures with increasing dimethylsilylene units, n, in the bridge. We found the electronic coupling between Si QDs and anchored

dimethylsilylene anthracenes in these hybrid systems is intermediate between our previously reported Si:9 EA and Si:9VA systems. By optimizing the surface density of tethered anthracene transmitters, the highest photon upconversion QY of 6.2% was obtained for Si:SiMe$_2$A with DPA as an emitter. As the dimethylsilylene units increase in the bridge, neither the photon upconversion QY or rate of triplet transfer show an exponential decay with increasing bridge length. Although we are limited by the capabilities of existing methods, our preliminary computational methods suggest this discrepancy is caused by dynamical structural fluctuations that modulate the spatial separation between Si QDs and surface-bound anthracene triplet acceptors. We hope this work stimulates ideas exploiting the conformational flexibility in oligosilanes for hybrid organic and inorganic nanostructures that show efficient long-range energy or charge transport.

Author contributions

S. G. L., K. W. and N. Q. N. made equal contributions. S. G. L. did the calculations; K. W. conducted the non-thermal plasma synthesis, the nanocrystal functionalization, photon upconversion, and ns-transient absorption (TA) experiments, N. Q. N., A. G. and T. C. S. performed the synthesis and characterization of molecular oligosilane copounds, H. W. the ultrafast TA spectroscopy; S. G. L., N. Q. N., K. W., T. A. S., L. M. and M. L. T. conceived of the project. S. G. L., and J. D. E. designed the calculations. S. G. L., K. W., J. D. E., T. A. S., M. L. T. and S. T. R. composed the manuscript with significant contributions from all authors.

Conflicts of interest

There are no conflicts to declare.

Data availability

Supplementary information (SI): additional figures, tables, notes, photophysical characterization, synthetic procedures and structural characterization, computational methods (PDF), *etc.* are available in the supplementary information. See DOI: https://doi.org/10.1039/d6sc00926c.

Acknowledgements

This work was partially supported by the U.S. National Science Foundation (CMMI-2053567 and CHE-2506109), the Air Force Office of Scientific Research (FA9550-25-1-0094, FA9550-23-1-0146), and the Cottrell Scholars Program (CS-CSA-2024-069). AG was supported by the UCR Chancellor's Research Fellowship. This work utilized the Alpine high performance computing resource at the University of Colorado Boulder. Alpine is jointly funded by the University of Colorado Boulder, the University of Colorado Anschutz, and Colorado State University and with support from NSF grants OAC-2201538 and OAC-2322260. We thank Mr. Fernando Alfaro and Mr. Imex Aguirre Cardenas (UC Riverside) for mass spectrometry characterization.

References

1 F. Strieth-Kalthoff, M. J. James, M. Teders, L. Pitzer and F. Glorius, Energy transfer catalysis mediated by visible light: principles, applications, directions, *Chem. Soc. Rev.*, 2018, **47**(19), 7190–7202, DOI: 10.1039/c8cs00054a.

2 K. Miyata, F. S. Conrad-Burton, F. L. Geyer and X. Y. Zhu, Triplet Pair States in Singlet Fission, *Chem. Rev.*, 2019, **119**(6), 4261–4292, DOI: 10.1021/acs.chemrev.8b00572.

3 Z. Y. Huang, T. Miyashita and M. L. Tang, Photon Upconversion at Organic-Inorganic Interfaces, *Annu. Rev. Phys. Chem.*, 2024, **75**, 329–346, DOI: 10.1146/annurev-physchem-090722-011335.

4 N. Yanai and N. Kimizuka, New Triplet Sensitization Routes for Photon Upconversion: Thermally Activated Delayed Fluorescence Molecules, Inorganic Nanocrystals, and Singlet-to-Triplet Absorption, *Acc. Chem. Res.*, 2017, **50**(10), 2487–2495, DOI: 10.1021/acs.accounts.7b00235.

5 T. W. Schmidt and F. N. Castellano, Photochemical Upconversion: The Primacy of Kinetics, *J. Phys. Chem. Lett.*, 2014, **5**(22), 4062–4072, DOI: 10.1021/jz501799m.

6 A. Monguzzi, R. Tubino, S. Hoseinkhani, M. Campione and F. Meinardi, Low power, non-coherent sensitized photon up-conversion: modelling and perspectives, *Phys. Chem. Chem. Phys.*, 2012, **14**(13), 4322–4332, DOI: 10.1039/c2cp23900k.

7 A. Neef, S. Beaulieu, S. Hammer, S. Dong, J. Maklar, T. Pincelli, R. P. Xian, M. Wolf, L. Rettig, J. Pflaum, *et al.*, Orbital-resolved observation of singlet fission, *Nature*, 2023, **616**(7956), 275, DOI: 10.1038/s41586-023-05814-1.

8 T. Ullrich, D. Munz and D. M. Guldi, Unconventional singlet fission materials, *Chem. Soc. Rev.*, 2021, **50**(5), 3485–3518, DOI: 10.1039/d0cs01433h.

9 S. S. Skourtis, C. Liu, P. Antoniou, A. M. Virshup and D. N. Beratan, Dexter energy transfer pathways, *Proc. Natl. Acad. Sci. U. S. A.*, 2016, **113**(29), 8115–8120, DOI: 10.1073/pnas.1517189113.

10 K. F. Wang, R. P. Cline, J. Schwan, J. M. Strain, S. T. Roberts, L. Mangolini, J. D. Eaves and M. L. Tang, Efficient photon upconversion enabled by strong coupling between silicon quantum dots and anthracene, *Nat. Chem.*, 2023, **15**(8), 1172, DOI: 10.1038/s41557-023-01225-x.

11 N. Nguyen, S. Lewis, K. Wang, H. Wang, A. Gonzalez, L. Mangolini, S. Roberts, M. Tang, J. Eaves and T. Su, Intermediate Electronic Coupling via Silane and Germane Bridges in Silicon Quantum Dot-Molecular Hybrid Systems, *Nano Lett.*, 2025, **25**(13), 5299–5306, DOI: 10.1021/acs.nanolett.5c00169.

12 X. Li, Z. Huang, R. Zavala and M. Tang, Distance-Dependent Triplet Energy Transfer between CdSe Nanocrystals and Surface Bound Anthracene, *J. Phys. Chem. Lett.*, 2016, **7**(11), 1955–1959, DOI: 10.1021/acs.jpclett.6b00761.

13 Z. Huang, Z. Xu, T. Huang, V. Gray, K. Moth-Poulsen, T. Lian and M. Tang, Evolution from Tunneling to Hopping

Mediated Triplet Energy Transfer from Quantum Dots to Molecules, *J. Am. Chem. Soc.*, 2020, **142**(41), 17581–17588, DOI: 10.1021/jacs.0c07727.

14 H. Wang, E. McNellis, S. Kinge, M. Bonn and E. Cánovas, Tuning Electron Transfer Rates through Molecular Bridges in Quantum Dot Sensitized Oxides, *Nano Lett.*, 2013, **13**(11), 5311–5315, DOI: 10.1021/nl402820v.

15 A. Morris-Cohen, M. Peterson, M. Frederick, J. Kamm and E. Weiss, Evidence for a Through-Space Pathway for Electron Transfer from Quantum Dots to Carboxylate-Functionalized Viologens, *J. Phys. Chem. Lett.*, 2012, **3**(19), 2840–2844, DOI: 10.1021/jz301318m.

16 T. Su, H. Li, R. Klausen, N. Kim, M. Neupane, J. Leighton, M. Steigerwald, L. Venkataraman and C. Nuckolls, Silane and Germane Molecular Electronics, *Acc. Chem. Res.*, 2017, **50**(4), 1088–1095, DOI: 10.1021/acs.accounts.7b00059.

17 W. Chen, J. Widawsky, H. Vázquez, S. Schneebeli, M. Hybertsen, R. Breslow and L. Venkataraman, Highly Conducting π-Conjugated Molecular Junctions Covalently Bonded to Gold Electrodes, *J. Am. Chem. Soc.*, 2011, **133**(43), 17160–17163, DOI: 10.1021/ja208020j.

18 R. MILLER and J. MICHL, POLYSILANE HIGH POLYMERS, *Chem. Rev.*, 1989, **89**(6), 1359–1410, DOI: 10.1021/cr00096a006.

19 T. Su, H. Li, M. Steigerwald, L. Venkataraman and C. Nuckolls, Stereoelectronic switching in single-molecule junctions, *Nat. Chem.*, 2015, **7**(3), 215–220, DOI: 10.1038/nchem.2180.

20 H. Tsuji, J. Michl and K. Tamao, Recent experimental and theoretical aspects of the conformational dependence of UV absorption of short chain peralkylated oligosilanes, *J. Organomet. Chem.*, 2003, **685**(1–2), 9–14, DOI: 10.1016/s0022-328x(03)00162-1.

21 P. Xia, E. K. Raulerson, D. Coleman, C. S. Gerke, L. Mangolini, M. L. Tang and S. T. Roberts, Achieving spin-triplet exciton transfer between silicon and molecular acceptors for photon upconversion, *Nat. Chem.*, 2020, **12**(2), 137–144, DOI: 10.1038/s41557-019-0385-8.

22 M. Montalti; S. L. Murov in. *Handbook of photochemistry*; CRC/Taylor & Francis, 2006. DOI: 10.1201/9781420015195.

23 T. Karatsu, T. Shibata, A. Nishigaki, K. Fukui and A. Kitamura, π–π and σ–π Interactions in α,ω-Dinaphthyl and -Dianthryl Oligosilanes in Solution, *Chem. Lett.*, 2003, **30**(10), 994–995, DOI: 10.1246/cl.2001.994.

24 T. Karatsu, Photochemistry and photophysics of organomonosilane and oligosilanes: Updating their studies on conformation and intramolecular interactions, *J. Photochem. Photobiol. C Photochem. Rev.*, 2008, **9**(3), 111–137, DOI: 10.1016/j.jphotochemrev.2008.06.001.

25 Z. Zhou, L. Gai, L.-W. Xu, Z. Guo and H. Lu, Disilane-bridged architectures: an emerging class of molecular materials, *Chem. Sci.*, 2023, **14**(38), 10385–10402, DOI: 10.1039/D3SC02690F.

26 U. R. Kortshagen, R. M. Sankaran, R. N. Pereira, S. L. Girshick, J. J. Wu and E. S. Aydil, Nonthermal Plasma Synthesis of Nanocrystals: Fundamental Principles, Materials, and Applications, *Chem. Rev.*, 2016, **116**(18), 11061–11127, DOI: 10.1021/acs.chemrev.6b00039.

27 M. P. Hanrahan, E. L. Fought, T. L. Windus, L. M. Wheeler, N. C. Anderson, N. R. Neale and A. J. Rossini, Characterization of Silicon Nanocrystal Surfaces by Multidimensional Solid-State NMR Spectroscopy, *Chem. Mater.*, 2017, **29**(24), 10339–10351, DOI: 10.1021/acs.chemmater.7b03306.

28 Z. Y. Yang, M. Iqbal, A. R. Dobbie and J. G. C. Veinot, Surface-Induced Alkene Oligomerization: Does Thermal Hydrosilylation Really Lead to Monolayer Protected Silicon Nanocrystals?, *J. Am. Chem. Soc.*, 2013, **135**(46), 17595–17601, DOI: 10.1021/ja409657y.

29 F. A. Reboredo, A. Franceschetti and A. Zunger, Excitonic transitions and exchange splitting in Si quantum dots, *Appl. Phys. Lett.*, 1999, **75**(19), 2972–2974.

30 M. Beard, K. Knutsen, P. Yu, J. Luther, Q. Song, W. Metzger, R. Ellingson and A. Nozik, Multiple exciton generation in colloidal silicon nanocrystals, *Nano Lett.*, 2007, **7**(8), 2506–2512, DOI: 10.1021/nl071486l.

31 M. Trinh, R. Limpens and T. Gregorkiewicz, Experimental Investigations and Modeling of Auger Recombination in Silicon Nanocrystals, *J. Phys. Chem. C*, 2013, **117**(11), 5963–5968, DOI: 10.1021/jp311124c.

32 B. Lee, J. Luo, N. Neale, M. Beard, D. Hiller, M. Zacharias, P. Stradins and A. Zunger, Quasi-Direct Optical Transitions in Silicon Nanocrystals with Intensity Exceeding the Bulk, *Nano Lett.*, 2016, **16**(3), 1583–1589, DOI: 10.1021/acs.nanolett.5b04256.

33 C. Stolle, X. Lu, Y. Yu, R. Schaller and B. Korgel, Efficient Carrier Multiplication in Colloidal Silicon Nanorods, *Nano Lett.*, 2017, **17**(9), 5580–5586, DOI: 10.1021/acs.nanolett.7b02386.

34 T. Huang, T. Koh, J. Schwan, T. Tran, P. Xia, K. Wang, L. Mangolini, M. Tang and S. Roberts, Bidirectional triplet exciton transfer between silicon nanocrystals and perylene, *Chem. Sci.*, 2021, **12**(19), 6737–6746, DOI: 10.1039/d1sc00311a.

35 D. DEXTER, A Theory Of Sensitized Luminescence In Solids, *J. Chem. Phys.*, 1953, **21**(5), 836–850, DOI: 10.1063/1.1699044.

36 A. Ronchi, C. Capitani, V. Pinchetti, G. Gariano, M. L. Zaffalon, F. Meinardi, S. Brovelli and A. Monguzzi, High Photon Upconversion Efficiency with Hybrid Triplet Sensitizers by Ultrafast Hole-Routing in Electronic-Doped Nanocrystals, *Adv. Mater.*, 2020, **32**(37), 2002953, DOI: 10.1002/adma.202002953.

37 A. Ronchi, P. Brazzo, M. Sassi, L. Beverina, J. Pedrini, F. Meinardi and A. Monguzzi, Triplet–triplet annihilation based photon up-conversion in hybrid molecule–semiconductor nanocrystal systems, *Phys. Chem. Chem. Phys.*, 2019, **21**(23), 12353–12359, DOI: 10.1039/C9CP01692A.

38 D. A. Rehn, C. W. Greeff, L. Burakovsky, D. G. Sheppard and S. D. Crockett, Multiphase tin equation of state using density functional theory, *Phys. Rev. B*, 2021, **103**(18), 184102, DOI: 10.1103/PhysRevB.103.184102.

39 G. Kresse and J. Furthmuller, Efficient iterative schemes for ab initio total-energy calculations using a plane-wave basis

set, *Phys. Rev. B:Condens. Matter Mater. Phys.*, 1996, **54**(16), 11169–11186.

40 D. M. Newns, Self-Consistent Model Of Hydrogen Chemisorption, *Phys. Rev.*, 1969, **178**(3), 1123.

41 P. W. Anderson, Localized Magnetic States In Metals, *Phys. Rev.*, 1961, **124**(1), 41.

42 D. L. Dexter, A Theory Of Sensitized Luminescence In Solids, *J. Chem. Phys.*, 1953, **21**(5), 836–850.

43 E. A. Weiss, G. Katz, R. H. Goldsmith, M. R. Wasielewski, M. A. Ratner, R. Kosloff and A. Nitzan, Electron transfer mechanism and the locality of the system-bath interaction: A comparison of local, semilocal, and pure dephasing models, *J. Chem. Phys.*, 2006, **124**(7), 074501, DOI: 10.1063/1.2168457.

44 D. Cadena, J. Sowa, D. Cotton, C. Wight, C. Hoffman, H. Wagner, J. Boette, E. Raulerson, B. Iverson, P. Rossky, *et al.*, Aggregation of Charge Acceptors on Nanocrystal Surfaces Alters Rates of Photoinduced Electron Transfer, *J. Am. Chem. Soc.*, 2022, **144**(49), 22676–22688, DOI: 10.1021/jacs.2c09758.

45 M. Sasaki, Y. Shibano, H. Tsuji, Y. Araki, K. Tamao and O. Ito, Oligosilane chain-length dependence of electron transfer of zinc porphyrin-oligosilane-fullerene molecules, *J. Phys. Chem. A*, 2007, **111**(16), 2973–2979, DOI: 10.1021/jp066749z.